Published in final edited form as:
Dev Dyn. 2011 March ; 240(3): 723–736. doi:10.1002/dvdy.22563.

GMAP210 AND IFT88 ARE PRESENT IN THE SPERMATID GOLGI APPARATUS AND PARTICIPATE IN THE DEVELOPMENT OF THE ACROSOME-ACROPLAXOME COMPLEX, HEAD-TAIL COUPLING APPARATUS AND TAIL

Abraham L. Kierszenbaum[1], **Eugene Rivkin**[1], **Laura L. Tres**[1], **Bradley K. Yoder**[2], **Courtney J. Haycraft**[2,*], **Michel Bornens**[3], and **Rosa M. Rios**[4]

[1]Department of Cell Biology and Anatomy, The Sophie Davis School of Biomedical Education, The City University of New York, New York NY 10031

[2]Department of Cell Biology, University of Alabama at Birmingham, School of Medicine, Birmingham, AL 35294

[3]Institut Curie, Compartimentation et Dynamique Cellulaires UMR144 CNRS-Institut Curie, 75248 Paris, France

[4]Department of Cell Signaling, Centro Andaluz de Biología, Molecular y Medicina Regenerativa, Edif. CARBIMER, 41092 Seville, Spain

Abstract

We describe the localization of the golgin GMAP210 and the intraflagellar protein IFT88 in the Golgi of spermatids and the participation of these two proteins in the development of the acrosome-acroplaxome complex, the head-tail coupling apparatus (HTCA) and the spermatid tail. Immunocytochemical experiments show that GMAP210 predominates in the *cis*-Golgi whereas IFT88 prevails in the *trans*-Golgi network. Both proteins co-localize in proacrosomal vesicles, along acrosome membranes, the HTCA and the developing tail. IFT88 persists in the acrosome-acroplaxome region of the sperm head whereas GMAP210 is not longer seen there. Spermatids of the *Ift88* mouse mutant display abnormal head shaping and are tail-less. GMAP210 is visualized in the *Ift88* mutant during acrosome-acroplaxome biogenesis. However, GMAP210–stained vesicles, mitochondria and outer dense fiber material build up in the manchette region and fail to reach the abortive tail stump in the mutant. *In vitro* disruption of the spermatid Golgi and microtubules with Brefeldin-A and nocodazole blocks the progression of GMAP210- and IFT88-stained proacrosomal vesicles to the acrosome-acroplaxome complex but F-actin distribution in the acroplaxome is not affected. We provide the first evidence that IFT88 is present in the Golgi of spermatids, that the microtubule-associated golgin GMAP210 and IFT88 participate in acrosome, HTCA and tail biogenesis, and that defective intramanchette transport of cargos disrupts spermatid tail development.

Send correspondence to: Dr. A. L. Kierszenbaum, Department of Cell Biology and Anatomy, The Sophie Davis School of Biomedical Education, 306 Harris Hall, 160 Convent Avenue, New York, NY 10031. Phone: (212) 650-6877. Fax: (212) 650-6812. kier@med.cuny.edu.
*Present address: Department of Medicine, Division of Nephrology, Medical University of South Carolina, Charleston, SC 29425

Keywords

acrosome; acroplaxome; microtubules; F-actin; intramanchette transport; intraflagellar transport

INTRODUCTION

Spermatids are highly polarized cells. Their structural polarity is determined by the opposite location of the acrosome-acroplaxome complex and the head-tail coupling apparatus (HTCA) with respect to the nucleus. Their functional polarity, aimed at the development of the head and tail of the future sperm, involves extracellular cues derived from Sertoli cells and the intracellular transport of protein complexes and organelles along microtubules and actin filament tracks. The Golgi apparatus, one of the landmarks of spermatid polarity, is the source of proacrosomal vesicles transported and tethering to the acroplaxome to form the acrosome. The acroplaxome is an F-actin-containing cytoskeletal plate with a keratin 5–containing desmosome-like marginal ring fastening the descending recess of the developing acrosome to the spermatid nuclear envelope (Kierszenbaum et al., 2003a; Kierszenbaum et al., 2007). Soon after acrosome biogenesis starts, a transient microtubule–containing manchette develops at the caudal site of the acrosome-acroplaxome complex. Like in somatic cells, the spermatid Golgi consists of stacks of closely apposed flatted membrane discs flanked by a cytomembrane network that serves as a cargo entry (*cis*-Golgi) site and a *trans*-Golgi network distribution site of proacrosomal vesicles. The fine structure and function of the spermatid Golgi have been described (reviewed in Clermont et al., 1993). The association of microtubules with the Golgi in spermatids has been documented by immunofluorescence microscopy (Moreno and Schatten, 2000). Still, the mechanism of proacrosomal vesicle transport is not completely understood. Two potential transporting routes have been proposed: (1) an F-actin cytoskeletal pathway involving the myosin Va/Rab27a/b complex (Kierszenbaum et al., 2003b) and (2) a microtubule cytoskeletal pathway involving the kinesin motor protein variant KIFC1 (Yang and Sperry, 2003). No clear understanding has surfaced to account for a dual cytoskeletal-based pathway during acrosome biogenesis. In addition, no general molecular mechanism has emerged thus far to account for the capture of proacrosomal vesicles and their microtubule-based transport leading to acrosome biogenesis.

The acrosome-acroplaxome complex, together with the manchette, play a significant role in sperm head shaping and the development of the HTCA and sperm tail during spermiogenesis (reviewed in Kierszenbaum and Tres, 2004; Kierszenbaum et al., 2007). The significance of the acrosome in fertilization is widely recognized. Accumulating evidence derived from transgenic mutants support the involvement of the acrosome-acroplaxome complex and the intramanchette transport of cargos in sperm modeling (Kierszenbaum, 2002). Because of the prominent contribution of the Golgi to acrosome biogenesis and the reported association of the intraflagellar protein IFT20 with GMAP210 (Follit et al., 2008), we are interested in determining the role in spermiogenesis of the coiled-coil protein GMAP210 (for Golgi-microtubule associated protein with a molecular mass of 210 kDa, Rios et al., 1994) and the intraflagellar transport (IFT) protein with a molecular mass of 88 kDa, designated IFT88 (also called Polaris, Murcia et al., 2000; Taulman et al., 2001).

Because it has been reported that IFT20 is the only IFT protein present in the Golgi (Follit et al., 2008), the presence of IFT88 in the spermatid Golgi is of interest.

GMAP210 was first identified as a *cis*-Golgi associated protein (Rios et al., 1994). GMAP210 relocates to the medial compartment in the presence of Brefeldin-A (Rios et al., 1994), co-purifies with microtubules (Infante et al., 1999; Kim et al., 2007), and, when over-expressed, breaks down the Golgi into aggregates of small vesicles (Pernet-Gallay et al., 2002) and perturbs the organization of the microtubule network (Infante et al., 1999). GMAP210 is necessary for maintaining the integrity of the Golgi ribbon (Rios et al., 2004; Yadav et al., 2009). The C-terminal region of GMAP210 contains a GRAB domain (GRIP-related Arf binding domain, Gillingham et al., 2004) that specifically binds flat membranes in an Arf1-dependent manner in *in vitro* assays (Drin et al., 2008). Yet, it is also likely that binding of the C-terminal region of GMAP210 to the *cis*-Golgi region is Arf12-independent and involves the participation of other factors (Cardenas et al., 2009). The N-terminal region contains an ALPS (amphipathic lipid-packing sensor) motif sensitive to membrane curvature (Drin et al., 2008). The structural characteristics of the terminal regions of the coiled-coil GMAP210 has led to a model in which membranes of spherical and flat curvature are tethered respectively to the N- and C-terminus of GMAP210 (Drin et al., 2008). This model could well fit a role of GMAP210 in the capture of spherical proacrosomal vesicles and their tethering to the outer acrosome membrane where membrane fusion occurs. The issue is to determine *in vivo* how does the coiled-coil GMAP210, with the GRAB and ALPS regions, associate with geometrically distinct vesicles and link to microtubules for vesicle transport.

It was initially described in flagella from *C. reinhardtii* cargos transported by a process called intraflagellar transport (Kozmisnski et al., 1993). Cargos are mobilized to the tip of a cilium along the microtubule axoneme by the kinesin-2 motor together with proteins of the intraflagellar transport-A (IFT-A) and IFT-B complexes. The dynein motor mediates the return of IFT cargo to the opposite direction (reviewed in Goetz and Anderson, 2010). IFT20, a member of the IFT-B complex, localizes in the Golgi as well in the cilium and interacts with a 163-amino acid cluster of the GMAP210 coiled-coil region (Follit et al., 2008). IFT20 is also visualized in the spermatid Golgi (Sironen et al., 2010). IFT20 is currently regarded as the only IFT protein present in the Golgi (Follit et al., 2008). In light of the known interaction of GMAP210 with IFT20 and their co-localization in the Golgi of somatic cells, it is relevant to determine whether GMAP210 is present in the Golgi of spermatids and its relationship with IFT88, another member of the IFT-B complex. Interest in GMAP210 derives from the report of neonatal lethal skeletal dysplasia in mice and achondrogenesis type 1A in humans, caused by a disruption in the Golgi architecture in multiple tissues of mice lacking GMAP210 (Smits et al., 2010). Interest in IFT88 derives from a ciliopathy phenotype in the Oak Ridge Polycystic Kidney (ORPK) mouse, caused by a hypomorphic mutation of the *Ift88* gene that impairs intraflagellar transport and development of the primary cilium (reviewed in Lehman et al., 2008). The Golgi and flagellum are two essential contributors of sperm development and their malfunction causes male infertility. The ORPK mouse is best known for its cystic renal phenotype and ciliary dysfunction (Pazour et al., 2000). The hypomorphic nature of the IFT88 allele in the ORPK mouse ($Ift88^{Tg737Rpw}$), designated here on for simplicity as *Ift88*, allows the homozygous

mutant mice to survive into early adulthood. The *Ift88* is a convenient model for analyzing the role of the protein IFT88 during spermatid development and for looking at the pleiotropic and idiopathic nature of clinical forms of male infertility.

We report here immunocytochemical observations supporting a role of GMAP210 and IFT88 in the microtubule-based transport of Golgi-derived vesicles during acrosome, HTCA and the tail biogenesis in spermatids. In the *Ift88* mutant mouse, GMAP210 and IFT88 co-localize in the acrosome-acroplaxome complex, but a disruption in the transporting function of the microtubule-containing manchette results in the build up of GMAP210– and myosin Va–stained cargos normally targeted to the HTCA and tail.

RESULTS

Transcript pattern and localization of GMAP210 in round spermatids

To obtain the necessary background information for testing the hypothesis that GMAP210 was involved in spermatid development, we analyzed the transcript pattern of GMAP210 in rat pachytene spermatocytes and spermatid cDNA expression libraries and in sperm and the immunolocalization of GMAP210 in spermatogenic cells. Figure 1, A shows GMAP210 transcripts in round spermatids but not in pachytene spermatocytes. Specific transcripts are also detected in sperm. Indirect immunofluorescence was used to determine the localization of GMAP210 in spermatogenic cells and correlate the findings with the RT-PCR data. Figure 1, B–F illustrates a cluster of mouse round spermatids and a single pachytene spermatocyte identified by its condensed XY chromosome pair. GMAP210 immunoreactivity is associated with the spermatid Golgi region and adjacent acrosome-acroplaxome complex (Figure 1, C). In agreement with the RT-PCR data, no GMAP210 immunoreactivity was detected in the pachytene spermatocyte. Figure 1, C shows that each spermatid displays a polarized GMAP210 immunoreactive region adjacent to the nucleus. An enlarged view (Figure 1, D) shows the strongly GMAP210 stained *cis*-Golgi continuous with the acrosome-acroplaxome perimeter capping the spermatid nucleus. The Golgi and acrosome were previously identified in similar spermatids preparations using specific markers (Kierszenbaum et al., 2003a; 2004b; Kierszenbaum et al., 2009). We concluded from these observations that GMAP210 transcripts and specific antigenic sites predominate in spermatids but not in spermatocytes and that GMAP210 localizes in the Golgi and the adjacent acrosome region.

Immunogold electron microscopy was used to precisely determine the GMAP210 subcellular localization in spermatids. Figure 2, A depicts the distribution sites of GMAP210 in a cross section of a rat spermatid (step 6), when acrosome development is in progress and the microtubule-containing manchette is not assembled. The plane of section of the cell is shown in a diagram (**inset,** Figure 2, A). GMAP210 predominates in the *cis*-Golgi and along the outer acrosome membrane and the inner acrosome membrane-acroplaxome complex. Neither the acrosome granule nor the acrosome contents are GMAP210 immunoreactive. Combined phase contrast-fluorescence microscopy of a similar spermatid developmental step shows a comparable GMAP210 immunostaining pattern (Figure 2, B–D) in agreement with the immunogold localization sites shown in Figure 2, A. A detailed immunogold electron microscopy view of the *trans*-Golgi network–acrosome interface shows the

association of GMAP210 with the surface of Golgi-derived proacrosomal vesicles and the outer and inner acrosome membrane, the latter closely apposed to the acroplaxome (Figure 2, E). These results suggested a role of GMAP210 in tethering proacrosomal vesicle to the acrosome and contributing GMAP210 to the membrane of the acrosomal sac.

Distribution sites of IFT88 in round spermatids

The presence of polaris/IFT88 in the spermatid manchette (Taulman et al., 2001) and the spermatid head (Kierszenbaum et al., 2004a) was previously reported. In contrast to GMAP210, IFT88 predominates in the *trans*-Golgi network region (Figure 2, F–H). Immunogold electron microscopy shows that IFT88 and GMAP210 are present at the cytosol side of proacrosomal vesicles adjacent to the *trans*-Golgi network and acrosome membranes (Figure 2, I). In agreement with GMAP210 localization, no IFT88 immunoreactivity was visualized in the medial Golgi region. The immunocytochemical data suggest that the initial co-localization of IFT88 with GMAP210 takes place in proacrosomal vesicles and that this co-localization persists following the merger of membrane stretches with the acrosomal membranes after proacrosomal vesicle tethering and fusion with the acrosome sac.

Localization of GMAP210 and IFT88 in elongating-mature spermatids and sperm and fractionated manchettes

Our next step was to determine the fate of GMAP210 and IFT88 immunoreactive sites during later steps of spermiogenesis, when spermatid shaping is in progress and the manchette develops just below the marginal ring of the acroplaxome. Indirect immunofluorescence of an elongating spermatid (rat, step 10 of spermiogenesis) reveals GMAP210 immmunoreactive sites at the acrosome-acroplaxome region and the manchette (Figure 3, A–B). Remarkably, manchettes fractionated by ultracentrifugation and stained with anti-β-tubulin (Figure 3, C) also displayed GMAP210 immunoreactivity (Figure 3, D), indicating the stability of GMAP210 following the manchette fractionation procedure (described in Mochida et al., 1998). Immunogold electron microscopy confirmed the presence of GMAP210 along the outer acrosomal membrane and the inner acrosomal membrane-acroplaxome site in a step 9-rat spermatid (Figure 3, E). During this spermiogenic step, the Golgi has already migrated to the caudal cytoplasmic region of the spermatid and F-actin-containing bundles at the Sertoli cell apical ectoplasmic region are closely apposed to the acrosome-acroplaxome complex. After the disassembly of the manchette in an elongated spermatid (step 16), GMAP210 is not longer seen in the acrosome-acroplaxome region. Instead, GMAP210 is visualized in the HTCA where the centrosome is present (Figure 3, F) and in the developing tail, including the axoneme and associated structures (Figure 3, v G). In contrast, GMAP210 immunoreactivity was stable in the HTCA and tail of the epididymal sperm (mouse, Figure 3, H–I).

IFT88 distribution in elongating spermatids and sperm showed similarities and differences with respect to GMAP210. First, the localization of IFT88 in the acrosome-acroplaxome complex and the manchette (**compare** Figure 3, E **with** Figure 4, A), fractionated manchettes (**compare** Figure 3, C–D **with** Figure 4, C–D) and sperm HTCA and tail (**compare** Figure 3, I **and** Figure 4, E–F) was equivalent to GMAP210. Figure 4, G shows

that the γ-tubulin staining of the HTCA in sperm correlates with IFT88 (Figure 4, F) and GMAP210 staining (see Figure 3, I). In contrast to GMAP210, IFT88 is visualized in the acrosome-acroplaxome complex in mouse (Figure 4, E) and rat (Figure 4, F) sperm. A section of rat seminiferous tubule (stage V of spermatogenesis) illustrates IFT88 immunoreactivity in the acrosome-acroplaxome region of step 5 round spermatids and step 17 elongated spermatids (Figure 4, B) but not in spermatogonia and pachytene spermatocytes. Essentially, GMAP210 and IFT88 co-localize in the acrosome-acroplaxome complex in round spermatids, but only IFT88 persisted in sperm in this location. Although the Golgi is prominent in pachytene spermatocytes, neither GMAP210 (Figure 1, F) nor IFT88 (Figure 4, B) are apparent. Furthermore, the relationship of GMAP210 and IFT88 with microtubules of isolated manchettes was strong enough to withstand the fractionation procedure. In summary, during the spermatid-to-sperm developmental transition, GMAP210 trans locates from the Golgi to the acrosome-acroplaxome to the manchette and then to the HTCA, where it localizes in the centrosome and the developing tail. The distribution sites of IFT88 in sperm are similar to GMAP210 except for the absence of GMAP210 in the acrosome-acroplaxome complex.

IFT88 localization sites in the *Ift88* hypomorphic mutant mouse

The immunocytochemical results suggested that GMAP210 and IFT88 participate in acrosome biogenesis and intramanchette transport of vesicles during spermatid development. Interest was then directed to the *Ift88* mutant mouse expressing a truncated form of IFT88. We concentrated on the developmental aspects of spermatids of the *Ift88* mutant because the relative number, structure, and developmental progression of spermatogonia and spermatocytes in the *Ift88* mutant were similar to the wild-type mouse. Transmission electron microscopy shows two relevant abnormalities: defects in spermatid head shaping and abortive tail development. Figure 5, A illustrates an elongating spermatid with dispersed mitochondria, microtubules and outer dense fiber material in the cytoplasm. An enlarged view (Figure 5, A, **inset**) shows randomly dispersed outer dense fibers associated with single microtubules without evidence of the axoneme-outer dense fiber typical organization. Figure 5, B depicts a spermatid tail stump with randomly arranged microtubules, two HTCA (instead of one as in wild-type spermatids) and three annulus spots (instead of two symmetric spots seen in sectioned wild-type spermatids). The inset in Figure 5, B illustrates a similar IFT88–stained *Ift88* mutant elongating spermatid showing an abortive tail stump. Most IFT88 immunofluorescence in elongating *Ift88* mutant spermatids resides in the acrosome-acroplaxome region and the abortive tail whereas β-tubulin is concentrated in the manchette and the tail stump (Figure 5, C–F). An analogous GMAP210 distribution is seen in *Ift88* mutant spermatids (Figure 5, G–J). A dotted GMAP210 staining pattern, regarded as vesicles, is seen in the manchette (Figure 6, H). The acroplaxome of an *Ift88* mutant spermatid with an abnormally shaped spermatid head displays a normal distribution of β-actin immunoreactivity (Figure 5, L). Transmission electron microscopy illustrates an *Ift88* mutant elongating spermatid with a distorted acrosome-acroplaxome complex, an ectopic assembled manchette and nuclear constriction at the subacrosomal region (Figure 5, M). Numerous vesicles are seen adjacent the microtubules of the manchette, in correlation with the GMAP–stained dotted pattern seen in Figure 5, H. Immunoblotitng experiments shows that the Ift88 antibody detects a strong immunoreactive

88 kDa protein band in wild-type testes, contrasting with a faint doublet in the *Ift88* mutant testes, consisting of 88 kDa and 85 kDa protein bands (Figure 5, N). The 88 kDa is regarded as the mature form of Ift88; the 85 kDa is probably the truncated form. Collectively, these observations indicated that spermatids of the *Ift88* mutant have a defect in nuclear shaping and severe abnormalities in the development of the HTCA and tail.

The myosin Va/Rab27 actin-based transport system in the *Ift88* mutant mouse

Previous studies showed the participation of the actin-based motor myosin Va in the transport of Rab27a/Rab27b-containing proacrosomal vesicles during acrosome biogenesis and vesicle intramanchette transport (Kierszenbaum et al., 2003b). Thus, we considered the possibility that a combined defect in the actin- and microtubule-based transport of cargos may occur in *Ift88* mutant spermatids. To obtain the necessary information for testing this hypothesis, we assessed whether components of the myosin Va-based transport system are transcribed in the testes of the *Ift88* mutant mouse. Figure 6, A shows similar transcript profiles of myosin Va, myosin VIIa, Rab27a and the adaptors melanophilin and MyRIP (for Myosin-Rab27a interacting protein) in wild-type and *Ift88* testes. Thus, at this level of analysis, the actin-based transport system in the *Ift88* mutant was regarded unchanged. An immunocytochemical evaluation of myosin Va distribution sites in *Ift88* mutant round spermatids shows proacrosomal vesicles clustered at the acrosome-acroplaxome pole (Figure 6, B). In turn, elongated spermatids of the *Ift88* mutant also display myosin Va-stained proacrosomal vesicles at the acrosome-acroplaxome region but a massive buildup of myosin-Va-stained vesicles at the caudal region of the manchette (Figure 6, C). The immunoreactive patterns of β-actin in the acroplaxome and manchette of round (Figure 6, D) and elongating spermatids (see Figure 5, K–L) in the *Ift88* mutant were comparable to wild-type spermatids (see Kierszenbaum et al., 2003b). We concluded that, although the components of the actin-based intramanchette transport system and GMAP210 were present, the occurrence of spermatid tail stumps could be attributed to the defective function of the truncated IFT88 protein in the *Ift88* mutant.

Nocodazol and Brefeldin-A disrupts the short-term dynamics of Golgi-derived proacrosomal vesicles

Early spermatids can recapitulate *in vitro* axoneme formation (Gerton and Millette, 1984; Mahr et al., 2003) but complete spermatid development and RNAi-mediated inhibition of gene expression have not been achieved. An alternative to study acrosome biogenesis is the use of specific mouse mutant models, such as the *Ift88* mutant. Another approach consists in short-term pharmacological *in vitro* experiments to analyze the sorting of Golgi-derived proacrosomal vesicles by disrupting microtubules with nocodazol (Moreno et al., 2006) or the endoplasmic reticulum-Golgi traffic with Brefeldin-A (Moreno et al., 2000). Bundles of microtubules in close association to the Golgi and acrosome in mouse round spermatids have been visualized by immunofluorescence (Moreno and Schatten, 2000). Figure 7, A–B and Figure 7, C–D show that exposure of rat round spermatids to nocodazol (10 μM for 2 hs) restricts GMAP210 and IFT88 immunoreactivity to the Golgi with a substantial decrease in fluorescence of the acrosome-acroplaxome complex, accompanied by a dotted-like spreading of IFT88 in the adjacent cytoplasm. A predominant GMAP210 and IFT88 immunofluorescent pattern is seen in the spermatid Golgi following Brefeldin-A treatment

(10 μg/ml for 20 min; Figure 7, F–G and Figure 7, H–I). β-Actin staining shows that neither nocodazole nor Brefeldin-A treatment dislocates the acrosome-acroplaxome complex from its nuclear anchoring site or alters the normal F-actin immunoreactive pattern (Figure 7, E and J). Spermatids exposed to the vehicle (DMSO or ethanol; negative control) display the characteristic GMAP210 and IFT88 Golgi to acrosome to acroplaxome sequence pattern (Figure 7, I–L). A recovery of the control immunofluorescent pattern is seen within 4 hs following rinsing and removal of nocodazol or Brefeldin-A from the incubation medium (not shown). We concluded from these experiments that the previously bound GMAP210 and IFT88 each separates rather rapidly from acrosome membrane binding sites in the presence of the pharmacologic agents and that dispersion of IFT88-containing material at the Golgi-acrosome region occurred in the presence of nocodazol. Yet, the attachment of the acrosome-acroplaxome complex to the spermatid nucleus and F-actin dynamics were not disrupted.

DISCUSION

We provide the first evidence that the golgin GMAP210 and the intraflagellar protein IFT88 participate in the development of the acrosome, centrosome and tail of spermatids. We also show that IFT88, like IFT20 (Follit et al., 2008), is an additional member of the IFT-B anterograde protein complex present in the Golgi. A molecular association of GMAP210 with the intraflagellar protein IFT20 has been reported (Follit et al., 2008). Whether GMAP210 and IFT88 are associated to each other needs to be determined. GMAP210 is seen at first in the *cis*-Golgi. IFT88 is initially detected in the *trans*-Golgi network. GMAP210 and IFT88 co-localize in the Golgi-derived proacrosomal vesicles. In epididymal sperm (rat and mouse), GMAP210 and IFT88 co-localize in the HTCA and tail. The presence of GMAP210 in the HTCA correlates with the ability of GMAP210 to interact with centrosomal γ-tubulin (Rios et al., 2004). Golgi membranes are largely confined to a region surrounding the centrosome or microtubule-organizing center and its aster of microtubules largely determines the positioning of the Golgi apparatus. IFT88 in the centrosome appears to be microtubule-independent and mediated by IFT88 tetratricopeptide repeat motif (Robert et al., 2007). Thus, GMAP210 and IFT88 in spermatids may enable the Golgi and centrosome to achieve a polarized geometry necessary for the correct and timely targeted delivery of cargos. Stabilized microtubules and F-actin and transporting proteins may facilitate Golgi positioning and the directional transport of cargos to the acrosome and the HTCA.

GMAP210 may have unique functions independent of IFTs and specific for spermatids during their development into sperm. Several observations support an IFT-independent role of GMAP210. First, we show that although GMAP210 and IFT88 persist in the sperm HTCA and tail, only IFT88 remains in the acrosome-acroplaxome region. Second, in the absence of GMAP210, the positioning of the Golgi is disrupted but the organization of the microtubule and actin networks appeared normal, demonstrating that Golgi positioning is critical in various aspects of cell polarity (Yadav et al., 2009). Third, a function of GMAP210 in fetal bone development is implied by the condition of neonatal fetal skeletal dysplasia in humans and mice lacking GMAP210 (Follit et al., 2008; Smits et al., 2010). Fourth, GMAP210 transcripts are expressed in spermatids but not in pachytene

spermatocytes, in agreement with the absence of specific immunoreactivity in spermatocytes, presumably denoting a negligible role of GMAP210 during meiosis.

Two relevant aspects of our work are the role of GMAP and IFT88 in acrosome biogenesis and tail development, and the functional significance of coexisting microtubule- and F-actin-based cargo transport systems. Concerning the first aspect, indirect immunofluorescence and immunogold electron microscopy show the co-localization of GMAP210 and IFT88 at the cytosol side of proacrosomal vesicles repositioning from the *trans*-Golgi network to the acrosome. The presence of GMAP210 and IFT88 along the outer and inner acrosome membranes indicates that Golgi-derived proacrosomal vesicles increase not only the acrosome content by delivering acrosomal proenzymes but also contribute stretches of membrane-associated GMAP210 and IFT88 (this work) and signaling proteins (Fer testis tyrosine kinase, Kierszenbaum et al., 2008; Fyn tyrosine kinase, Kierszenbaum et al., 2009). A disruption of the Golgi and microtubule function in round spermatids following treatments with Brefeldin-A and nocodazole, respectively, appears to disrupt the stability and progression of GMAP210 and IFT88 in the acrosome-acroplaxome complex. Yet, defective IFT88 in the *Ift88* mutant does not disrupt acrosome-acroplaxome biogenesis. Thus, the integrity of the Golgi and microtubule network is a requirement for the normal progression of acrosome-acroplaxome biogenesis. The fetal lethality of the *GMAP210* mutant (Follit et al., 2008) prevents determination of a specific role of GMAP210 in acrosome-acroplaxome biogenesis.

An understanding of the role of the GMAP210 and IFT88 during acrosome-acroplaxome biogenesis and intramanchette transport of cargos depends on determining whether these two proteins interact with each other and how each of them associates with Golgi-derived vesicles and microtubules. Concerning the first aspect, further biochemical studies are required to determine whether GMAP210 with IFT88 associate with each other and, if so, which specific region of IFT88 associates with GMAP210. Regarding the second aspect, *in vitro* studies have led to propose a model in which the N-terminus of GMAP210 tethers to curved membranes and the C-terminus to less curved membranes to capture small transport vesicles at the endoplasmic reticulum-Golgi interface (Drin et al., 2008). Although the proposed model of membrane binding, based on the detection of membrane curvature, may be relevant to GMAP210 function during acrosome biogenesis, further studies should determine whether the proposed model applies to the *in vivo* situation.

GMAP210, like several other Golgi-localized proteins categorized as tethering golgins, displays a coiled-coil rod domain with a potential hinge region. Available data support the view that GMAP210 has at least two membrane targeting motifs bridged by the long coiled-coil domain, which in several golgins has a length ranging from 50 to 300 nm (Sztul and Lupashin, 2006). Since the membrane of proacrosomal vesicles captured by GMAP210 must be close enough to the outer acrosomal membrane to permit fusion, the hinge region may collapse the tether to bring the membranes into proximity to allow Hrb- (Kang-Decker et al., 2001; Kierszenbaum et al., 2004b) or SNARE-dependent vesicle–acrosome fusion (Ramalho-Santos et al., 2001). Significantly, Hrb has an N-terminal Arf-GAP domain, thus emphasizing the role of G proteins during acrosome biogenesis. Another alternative, independent of the geometry of proacrosomal vesicles, is that GMAP210 may bind to an

interacting partner on the proacrosomal vesicle. Rab-family small GTPases associated to a vesicle membrane may interact with a site proximal to the GRAB domain of GMAP210 or any other golgin. Although members of the Rab-family of small GTPases are found in the acrosome (Rab3a, Iida et al., 1999; Rab27a/Rab27b, Kierszenbaum et al., 2003b), there is no evidence that GMAP210 can establish partnership with known acrosomal Rab proteins.

Historically, microtubules and their associated motor and non-motor proteins have been linked to trafficking at the Golgi and from the Golgi to the acrosome (Moreno and Schatten, 2006; Yang and Sperry, 2003). There is evidence that the actin-based motor myosin Va, interacting with Rab27a/Rab27b in proacrosomal vesicles, also participate in acrosome biogenesis (Kierszenbaum et al., 2003b). The *Ift88* mouse mutant, expressing defective IFT88 but an intact myosin Va-Rab27a/Rab27b actin-based vesicle transport system, provides clues on how the microtubule- and actin-based transport systems might contribute to acrosome-acroplaxome and tail biogenesis. The development of the acrosome-acroplaxome complex is not significantly disrupted in the *Ift88* mutant. Although the actin-based transport system may partially offset the deficiency of the microtubule-based transport system and defective IFT88 protein, such compensation does not appear to override abnormal spermatid head shaping. Like myosin Va and Rab27/Rab27b, GMAP210 and IFT88 appear to participate in the intramanchette transport of cargos to the HTCA and the tail. GMAP210 and IFT88 are tightly linked to microtubules of the manchette as inferred by their endurance following manchette fractionation by density gradient ultracentrifugation. Whether the incorrectly assembled microtubule tracks or variations in the type and amount of post-translationally modified tubulin isoforms in the manchette (Mochida et al., 1999) may influence the alignment and transporting function of companion actin tracks in the manchette needs to be determined.

In summary, this work shows that GMAP210 and IFT88 localize in distinct Golgi regions and co-localize at the cytosol side of Golgi-derived proacrosomal vesicles, acrosome membranes, and the HTCA of mouse and rat spermatids, and that a pharmacological disruption of Golgi and microtubule function arrests the progression of acrosome-acroplaxome development. In the *Ift88* mutant mouse, the development of the acrosome-acroplaxome complex appears undisturbed but a severe arrest in the transport of cargos along the microtubule-containing manchette results in the development of tail-less spermatids. Based on the GMAP210 knockdown phenotype, showing Golgi dispersal (Rios *et al.*, 2004), experiments affecting Golgi positioning without disrupting secretion or the organization of the actin and microtubule networks (Yadav et al., 2009), and the *Ift88* mutant spermatid phenotype (this work), we propose that GMAP210 contributes to spermatid Golgi-centrosome positioning, a condition required for normal acrosome biogenesis, and to the accurate delivery of cargos by intramanchette transport to the HTCA, involving microtubule-based IFT88 and the F-actin-myosin Va transport system. Our observations open new molecular perspectives to understand the role of GMAP210 and IFT88 in sperm development leading to the clinical characterization of pleiotropic or idiopathic causes of male infertility.

EXPERIMENTAL PROCEDURES

RT-PCR and immunoblotting

Reverse transcriptase-polymerase chain reaction (RT-PCR) analysis was used to identify specific transcripts of adult rat (Sprague-Dawley) and mouse (adult wild-type and 24–28-day old *Ift88* mutant) testis, epididymal rat sperm, rat pachytene spermatocytes, and round spermatids cDNA expression libraries. Total RNA from rat and mouse testis was prepared using TRI Reagent (MRC, Cincinnati, OH). Single stranded cDNAs was synthesized using a Superscript III kit (Invitrogen, Carlsbad, CA). PCR was performed on GenAmp 2700 system (Applied Biosystems, Foster City, CA) using Go Taq DNA Polymerase (Promega, Madison, WI). Standard conditions included incubation of PCR reactions at 94°C/2.5min followed by 40 cycles of 94°C/10sec, 58–61°C/10sec, 72°C/45sec.The sequence of the used forward and reverse primers for rat and mouse are indicated in Table 1. Technical details of the construction of rat pachytene and round spermatid cDNA expression libraries were reported (Rivkin et al., 1997). The procedure for extraction of total RNA of testis and epididymal sperm was described (Kierszenbaum et al., 2008).

An immunogenic peptide from rat and mouse IFT88/polaris was selected using a protein analysis program (Protean, DNASTAR, Madison, WI). A peptide with the sequence $_{209}$EIDEDDKYISPSDDPH$_{224}$ was synthesized, the amino acid sequence verified by mass spectrometry and used for rabbit immunization according to a standard immunization protocol (Sigma Genosys, The Woodlands, TX). The specificity of anti-IFT88 serum was determined by immunoblotting using lysates of rat testis (adult, Sprague-Dawley) and absorption of the antibody with the antigenic peptide. Immunoblotting was carried out as previously described (Kierszenbaum et al., 2003a). The specificity and characteristics of the anti-GMAP210 polyclonal serum generated in rabbits were reported (Infante et al., 1999).

Indirect immunofluorescence and immunogold electron microscopy

Spermatogenic cells and epididymal sperm from adult rats and spermatogenic cells from *Ift88* mutant and wild-type mice were collected from seminiferous tubular fragments and cauda epididymis as reported (Kierszenbaum et al., 2003a). Rat spermatogenic stages were identified using a dissecting stereomicroscope to visualize specific transillumination patterns of the tubular fragments. Dispersed spermatogenic cells were fixed for 15 min by adding a drop of 3.7% paraformaldehyde (electron microscopy grade) in 0.1 M sucrose in phosphate buffer, pH 7.4, on microscope slides coated with Vectabond (Vector Laboratories, Burlingame, CA). This fixation procedure yields plasma membrane-free preparations in which the spermatid nucleus with associated Golgi, acrosome, acroplaxome, manchette, chromatoid body, and HTCA can be readily visualized. Antibodies to β-tubulin and anti-β-actin (1:100; Sigma, St. Louis, MO), anti–γ-tubulin (1:50; catalog number T6557; Sigma), myosin Va (1:50; catalog no. AB5887P; Chemicon International, Temecula, CA) were used to localize the manchette, acroplaxome, centrioles, and Golgi-derived proacrosomal vesicles, respectively. Cells were immunoreacted with anti-GMAP210 rabbit serum (working dilution, 1:1000) and anti-IFT88 rabbit serum (working dilution, 1:500). Preimmune serum and preabsorbed antiserum with antigenic peptide were used as controls (data not shown).

Second antibodies were Alexa Fluor-conjugated goat anti-rabbit and anti-mouse IgG (working dilution, 1:200; Molecular Probes, Eugene, OR). Specimens were mounted with Vectashield (Vector Laboratories) without or with propidium iodide (to detect nucleic acids by a red emission color). Specimens were observed using a fluorescence microscope equipped with episcopic illumination. Images were recorded using a Magnafire digital camera (Optronics, Goleta, CA).

For transmission electron microscopy, rat and mouse (wild-type and *Ift88* mutant) testes were fixed and processed as described (Kierszenbaum et al., 2003a). For immunogold electron microscopy, testes from adult rats were fixed in a mixture of 1.5% glutaraldehyde and 3.4% paraformaldehyde (electron microscope grade) in 0.1 M phosphate buffer, pH 7.2, embedded in Lowicryl K4M (Polysciences, Warrington, PA), and processed for immunogold microscopy as described previously (Rivkin et al., 1997). Anti-GMAP210 and anti-IFT88 were used at working dilutions of 1:100 in phosphate-buffered saline containing 0.1% Tween 20, 1% bovine serum albumin, and 1% goat serum. Bound antibody was detected by incubating the sample overnight at 4°C with goat anti-rabbit IgG conjugated with 10-nm gold particles (Amersham Biosciences, Piscataway, NJ) by using a 1:25 working dilution. Thin sections were stained for 5 min with 5% uranyl acetate in deionized water, and specimens were examined using a JEM-100CX transmission electron microscope operated at an accelerating voltage of 60 kV. Thick sections (1–2 μm thick) of testis embedded in Lowicryl were stained with anti-IFT88 serum as reported (Kierszenbaum et al., 2003b) and examined using a fluorescence microscope.

Treatment of spermatids with nocodazole and Brefeldin-A

Spermatogenic-stage specific rat seminiferous tubules (stages V–VII) were selected by their transillumination pattern and collected in serum-free Minimum Essential Medium with Earle salts and lacking phenol red culture medium as reported (Kierszenbaum et al., 2003a). Spermatogenic cells, mainly spermatids (steps 5–7 of spermiogenesis) and spermatocytes (predominantly pachytene spermatocytes) in the isolated seminiferous tubules were dispersed mechanically in culture medium by touching repeatedly the air-culture medium interface. Tissue culture-treated BD Falcon 96-well plates (320 μl volume/well) were used. The culture medium contained either nocodazole (10 μM; Sigma; Cat. M1404) or Brefeldin-A (10 μg/ml; Sigma; Cat. B7651). Samples were incubated at 34°C in nocodazole for 2 hs and Brefeldin-A for 20 min. Controls included culture medium containing vehicle (DMSO or ethanol). Cells were collected with glass pipette, placed on a Vectabond coated microscope slides, fixed as described above for dispersed cells and processed for indirect immunofluorescence using GMAP210, IFT88 and β-actin antibodies. In some experiments, the drug-containing medium was carefully removed with a micropipette, cells washed twice with drug-free culture medium and incubated for an additional 4-h period. Cells were processed for indirect immunofluorescence as indicated above.

Acknowledgments

We thank Drs. Jovenal T. San Agustin and George Witman for sharing with one of us (ALK) electron microscopy data of the *Ift88* mutant mouse testis. Supported in part by NIH HD36477 (LLT), DK065655 (BKY), and HD37282 (ALK) grants.

REFERENCES

Ali MY, Krementsova EB, Kennedy GG, Mahaffy R, Pollard TD, Trybus KM, Warshaw DM. Myosin Va maneuvers through actin intersections and diffuses along microtubules. Proc Natl Acad Sci U S.A. 2007; 104:4332–4336. [PubMed: 17360524]

Cardenas J, Rivero S, Goud B, Bornens M, Rios RM. Golgi localisation of GMAP210 requires two distinct cis-membrane binding mechanisms. BMC Biol. 2009; 7:56. [PubMed: 19715559]

Clermont, Y.; Oko, R.; Hermo, L. Cell biology of mammalian spermiogenesis. In: Desjardins, C.; Ewing, LL., editors. Cell and molecular biology of the testis. New York: Oxford University Press; 1993. p. 332-376.

Drin G, Morello V, Casella JF, Gounon P, Antonny B. Asymmetric tethering of flat and curved membranes by a golgin. Science. 2008; 320:670–673. [PubMed: 18451304]

Follit JA, San Agustin JT, Xu F, Jonassen JA, Samtani R, Lo CW, Pazour GJ. The Golgin GMAP210/TRIP11 anchors IFT20 to the Golgi complex. PLoS Genet. 2008; 4:e1000315. [PubMed: 19112494]

Gerton GL, Millette CF. Generation of flagella by cultured mouse spermatids. J Cell Biol. 1984; 98:619–628. [PubMed: 6363426]

Gillingham AK, Tong AH, Boone C, Munro S. The GTPase Arf1p and the ER to Golgi cargo receptor Erv14p cooperate to recruit the golgin Rud3p to the cis-Golgi. J Cell Biol. 2004; 167:281–292. [PubMed: 15504911]

Goetz SC, Anderson KW. The primary cilium: a signaling centre during vertebrate development. Nat Rev Genet. 2010; 11:331–344. [PubMed: 20395968]

Iida H, Yoshinaga Y, Tanaka S, Toshimori K, Mori T. Identification of Rab3A GTPase as an acrosome-associated small GTP-binding protein in rat sperm. Dev Biol. 1999; 211:144–155. [PubMed: 10373312]

Infante C, Ramos-Morales F, Fedriani C, Bornens M, Rios RM. GMAP210, A cis-Golgi network-associated protein, is a minus end microtubule-binding protein. J Cell Biol. 1999; 145:83–98. [PubMed: 10189370]

Kang-Decker N, Mantchev GT, Juneja SC, McNiven MA, van Deursen JM. Lack of acrosome formation in Hrb-deficient mice. Science. 2001; 294:1531–1533. [PubMed: 11711676]

Kierszenbaum AL. Intramanchette transport (IMT): managing the making of the spermatid head, centrosome, and tail. Mol. Reprod Dev. 2002; 63:1–4. [PubMed: 12211054]

Kierszenbaum AL, Rivkin E, Talmor-Cohen A, Shalgi R, Tres LL. Expression of full-length and truncated Fyn tyrosine kinase transcripts and encoded protein during spermatogenesis and localization during acrosome biogenesis and fertilization. Mol Reprod Dev. 2009; 76:832–843. [PubMed: 19441121]

Kierszenbaum AL, Rivkin E, Tres LL. Acroplaxome, an F-actin-keratin-containing plate, anchors the acrosome to the nucleus during shaping of the spermatid head. Mol Biol Cell. 2003a; 14:4628–4640. [PubMed: 14551252]

Kierszenbaum AL, Rivkin E, Tres LL. The actin-based motor myosin Va is a component of the acroplaxome, an acrosome-nuclear envelope junctional plate, and of manchette-associated vesicles. Cytogenet Genome Res. 2003b; 103:337–344. [PubMed: 15051957]

Kierszenbaum AL, Rivkin E, Tres LL. Molecular biology of sperm head shaping. Soc Reprod Fertil Suppl. 2007; 65:33–43. [PubMed: 17644953]

Kierszenbaum AL, Rivkin E, Tres LL. Expression of Fer testis (FerT) tyrosine kinase transcript variants and distribution sites of FerT during the development of the acrosome-acroplaxome-manchette complex in rat spermatids. Dev Dyn. 2008; 237:3882–3891. [PubMed: 18985748]

Kierszenbaum AL, Tres LL. The acrosome-acroplaxome-manchette complex and the shaping of the spermatid head. Arch Histol Cytol. 2004; 67:271–284. [PubMed: 15700535]

Kierszenbaum AL, Tres LL, Rivkin E, Haycraft CJ, Yoder BK. Disrupted intramanchette and intraflagellar cargo transport in spermatids of the orpk mutant mouse. Mol Biol Cell. 2004a; 15:132a. [PubMed: 14565984]

Kierszenbaum AL, Tres LL, Rivkin E, Kang-Decker N, van Deursen JM. The acroplaxome is the docking site of Golgi-derived myosin Va/Rab27a/b- containing proacrosomal vesicles in wild-type and Hrb mutant mouse spermatids. Biol. Reprod. 2004b; 70:1400–1410. [PubMed: 14724135]

Kim HS, Takahashi M, Matsuo K, Ono Y. Recruitment of CG-NAP to the Golgi apparatus through interaction with dynein-dynactin complex. Genes Cells. 2007; 12:421–434. [PubMed: 17352745]

Kozminski KG, Johnson KA, Forscher P, Rosenbaum JL. A motility in the eukaryotic flagellum unrelated to flagellar beating. Proc Nat Acad Sci USA. 1993; 90:5519–5523. [PubMed: 8516294]

Lehman JM, Michaud EJ, Schoeb TR, Aydin-Sun Y, Miller M, Yoder BK. The Oak Ridge Polycystic kidney mouse: Modeling ciliopathies of mice and men. Dev Dyn. 2008; 237:1960–1971. [PubMed: 18366137]

Mahr J, Tres LL, Yamazaki Y, Yanagimachi R, Kierszenbaum AL. Mouse round sspermatids developed in vitro from preexisting spermatocytes can produce normal offspring by nuclear injection in to in vivo-developed mature oocytes. Biol Reprod. 2003; 69:169–176. [PubMed: 12620938]

Mochida K, Tres LL, Kierszenbaum AL. Isolation of the rat spermatid manchette and its perinuclear ring. Dev Biol. 1998; 200:46–56. [PubMed: 9698455]

Mochida K, Tres LL, Kierszenbaum AL. Structural and biochemical features of fractionated spermatid manchettes and sperm axonemes of the azh/azh mutant mouse. Mol Reprod Dev. 1999; 52:434–444. [PubMed: 10092124]

Moreno RD, Palomino J, Schatten G. Assembly of spermatid acrosome depends on microtubule organization during mammalian spermiogenesis. Dev Biol. 2006; 293:218–227. [PubMed: 16540102]

Moreno RD, Ramalho-Santos J, Sutovsky P, Chan EK, Schatten G. Vesicular traffic and Golgi apparatus dynamics during mammalian spermatogenesis: implications for acrosome architecture. Biol Reprod. 2000; 63:89–98. [PubMed: 10859246]

Moreno RD, Schatten G. Microtubule configurations and post-translational alpha-tubulin modifications during mammalian spermatogenesis. Cell Motil Cytoskeleton. 2000; 46:235–246. [PubMed: 10962478]

Murcia NS, Richards WG, Yoder BK, Mucenski ML, Dunlap JR, Woychik RP. The Oak Ridge Polycystic Kidney (orpk) disease gene is required for left-right axis determination. Development. 2000; 127:2347–2355. [PubMed: 10804177]

Pazour GJ, Dickert BL, Vucica Y, Seeley ES, Rosenbaum JL, Witman GB, Cole DG. Chlamydomonas IFT88 and its mouse homologue, polycystic kidney disease gene tg737, are required for assembly of cilia and flagella. J Cell Biol. 2000; 151:709–718. [PubMed: 11062270]

Pernet-Gallay K, Antony C, Johannes L, Bornens M, Goud B, Rios RM. The overexpression of GMAP210 blocks anterograde and retrograde transport between the ER and the Golgi apparatus. Traffic. 2002; 3:822–832. [PubMed: 12383348]

Ramalho-Santos J, Moreno RD, Wessel GM, Chan EK, Schatten G. Membrane trafficking machinery components associated with the mammalian acrosome during spermiogenesis. Exp Cell Res. 2001; 267:45–60. [PubMed: 11412037]

Rios RM, Tassin AM, Celati C, Antony C, Boissier MC, Homberg JC, Bornens M. A peripheral protein associated with the cis-Golgi network redistributes in the intermediate compartment upon Brefeldin A treatment. J Cell Biol. 1994; 125:997–1013. [PubMed: 8195302]

Rios RM, Sanchis A, Tasin AM, Feedriani C, Bornens M. GMAP-210 recruits γ-tubulin complexes to cis-Golgi membranes and is required for Golgi ribbon formation. Cell. 2004; 118:323–335. [PubMed: 15294158]

Rivkin E, Cullinan EB, Tres L, Kierszenbaum AL. A protein associated with the manchette during rat spermiogenesis is encoded by a gene of the TBP-1-like subfamily with highly conserved ATPase and protease domains. Mol Reprod Dev. 1997; 48:77–89. [PubMed: 9266764]

Robert A, Margall-Ducos G, Guidotti JE, Brégerie O, Celati, Bréchot C, Desdouets C. The intraflagellar transport component IFT88/polaris is a centrosomal protein regulating G1-S transition in non-ciliated cell. J Cell Sci. 2007; 120:628–637. [PubMed: 17264151]

Sinka R, Gillingham AK, Kondylis V, Munro S. Golgi coiled-coil proteins contain multiple binding sites for Rab family G proteins. J Cell Biol. 2008; 183:607–615. [PubMed: 19001129]

Smits P, Bolton AD, Funari V, Hong M, Boyden ED, Lu L, Manning DK, Dwyer ND, Moran JL, Prysak M, Merriman B, Nelson SF, Bonafé L, Superti-Furga A, Ikegawa S, Krakow D, Cohn DH,

Kirchhausen T, Warman ML, Beier DR. Lethal skeletal dysplasia in mice and humans lacking the golgin GMAP210. N Engl J Med. 2010; 362:206–216. [PubMed: 20089971]

Sironen A, Hansen J, Thomsen B, Andersson M, Vilkki J, Toppari J, Kotaja N. Expression of SPEF2 during mouse spermatogenesis and identification of IFT20 as an interacting protein. Biol Reprod. 2010; 82:580–590. [PubMed: 19889948]

Sztul E, Lupashin V. Role of tethering factors in secretory membrane traffic. Am J Physiol Cell Physiol. 2006; 290:C11–C26. [PubMed: 16338975]

Taulman PD, Haycraft CJ, Balkovetz DF, Yoder BK. Polaris, a protein involved in left-right axis patterning, localizes to basal bodies and cilia. Mol Biol Cell. 2001; 12:589–599. [PubMed: 11251073]

Yadav S, Puri S, Linstedt AD. A primary role for Golgi positioning in directed secretion, cell polarity, and wound healing. Mol Biol Cell. 2009; 20:1728–1736. [PubMed: 19158377]

Yang WX, Sperry AO. C-terminal kinesin motor KIFC1 participates in acrosome biogenesis and vesicle transport. Bio. Reprod. 2003; 69:1719–1729. [PubMed: 12826589]

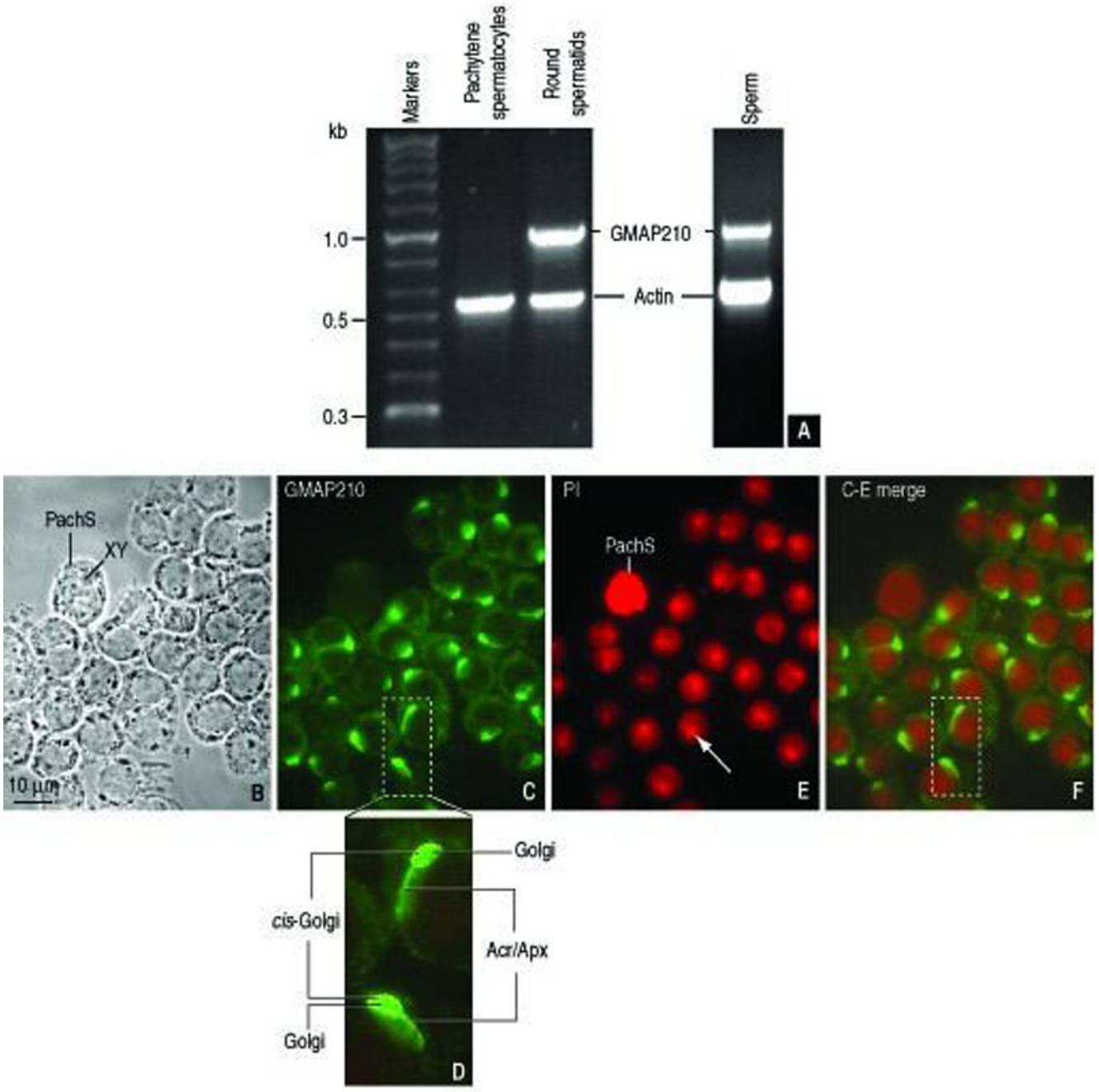

FIGURE 1.

GMAP210 transcripts and immunolocalization. **A**. GMAP210 transcripts detected by RT-PCR in a rat round spermatid cDNA expression library and rat epididymal sperm but not in a rat pachytene spermatocytes cDNA expression library. **B**: Phase-contrast microscopy of round spermatids and a single pachytene spermatocyte with the characteristic XY chromosomal condensed mass. **C**. Immunofluorescent localization of GMAP210 in spermatids but not in the pachytene spermatocytes. **D**. Enlarged view of the **dashed box** of panel **C**. GMAP210 immunoreactivity is detected at the *cis*-Golgi and extending in a comet-

like fashion to the acrosome-acroplaxome region. **E**. Propidium iodide (**PI**) nucleic acid staining showing the characteristic densely stained chromocenter in round spermatid nuclei (**arrow**) contrasting with the intense chromosomal staining in the pachytene spermatocytes. **F**. C-E merge image. The **dashed box** corresponds to the enlarged view shown in panel D.

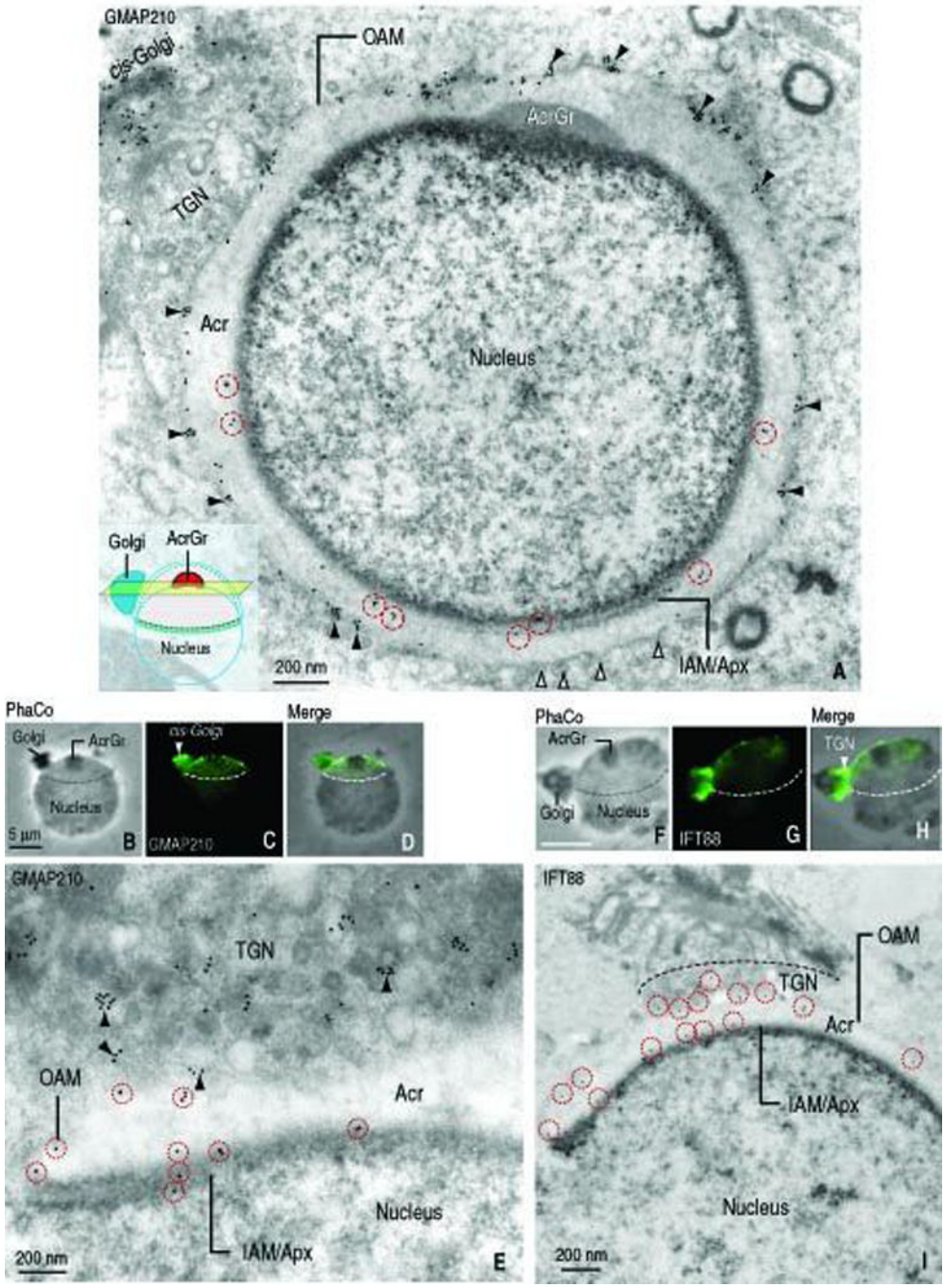

FIGURE 2.

Localization of GMAP210 and IFT88 in round spermatids (rat; step 6) by immunogold electron microscopy and indirect immunofluorescence. **A**. Immunogold electron microscopy shows GMAP210 immunoreactive sites at the *cis*-Golgi and at the outer acrosome membrane (**OAM, arrowheads**) and inner acrosome membrane-acroplaxome interface (**IAM/Apx**) of a round spermatid. The diagram in the inset indicates the plane of the cross-section. Gold particles along the IAM/Apx surface are denoted by a **dashed red circle**. The **open arrowheads** indicate fusing vesicles. **B–D**: Panel B is a phase-contrast (**PhaCo**)

microscopy image showing the Golgi, the acrosome granule (**AcrGr**) and the nucleus. Panel C shows the GMAP210 stained Golgi, predominantly at the *cis*-Golgi region, and the acrosome-acroplaxome complex. The **dashed line** indicated the caudal margin of the acrosome-acroplaxome complex. Panel D is the merge of panels B and C. **E**. Detailed view of the *trans*-Golgi-acrosome-acroplaxome region displaying immunogold GMAP210 sites along the wall of proacrosomal vesicles (**arrowheads**), the outer acrosome membrane (**OAM**) and the inner acrosome membrane-acroplaxome interface (**IAM/Apx**). Gold particles along the acrosome membranes are indicated by a **red dashed circle. F–H**. Indirect immunofluorescence of IFT88 (panel G). Unlike GMAP210 predominant localization in *cis*-Golgi (panel C), IFT88 is restricted to the *trans*-Golgi. Similar to GMAP210, specific immunoreactivity extends to the acrosome-acroplaxome complex (panel F, phase contrast microscopy (**PhaCo**) displaying the position of the Golgi with respect to the nucleus and the acrosome granule (**AcrGr**) and panel H (merge of panels F and G). The boundary of the acrosome-acroplaxome complex is denoted by the **dashed line. I**. Immunogold electron microscopy localization of IFT88 in the *trans*-Golgi, along the outer acrosome membrane (**OAM**) and the inner acrosome-acroplaxome interface (**IAM/Apx**). Gold particles along the acrosome membranes are indicated by **red dashed circles. Acr**, acrosome.

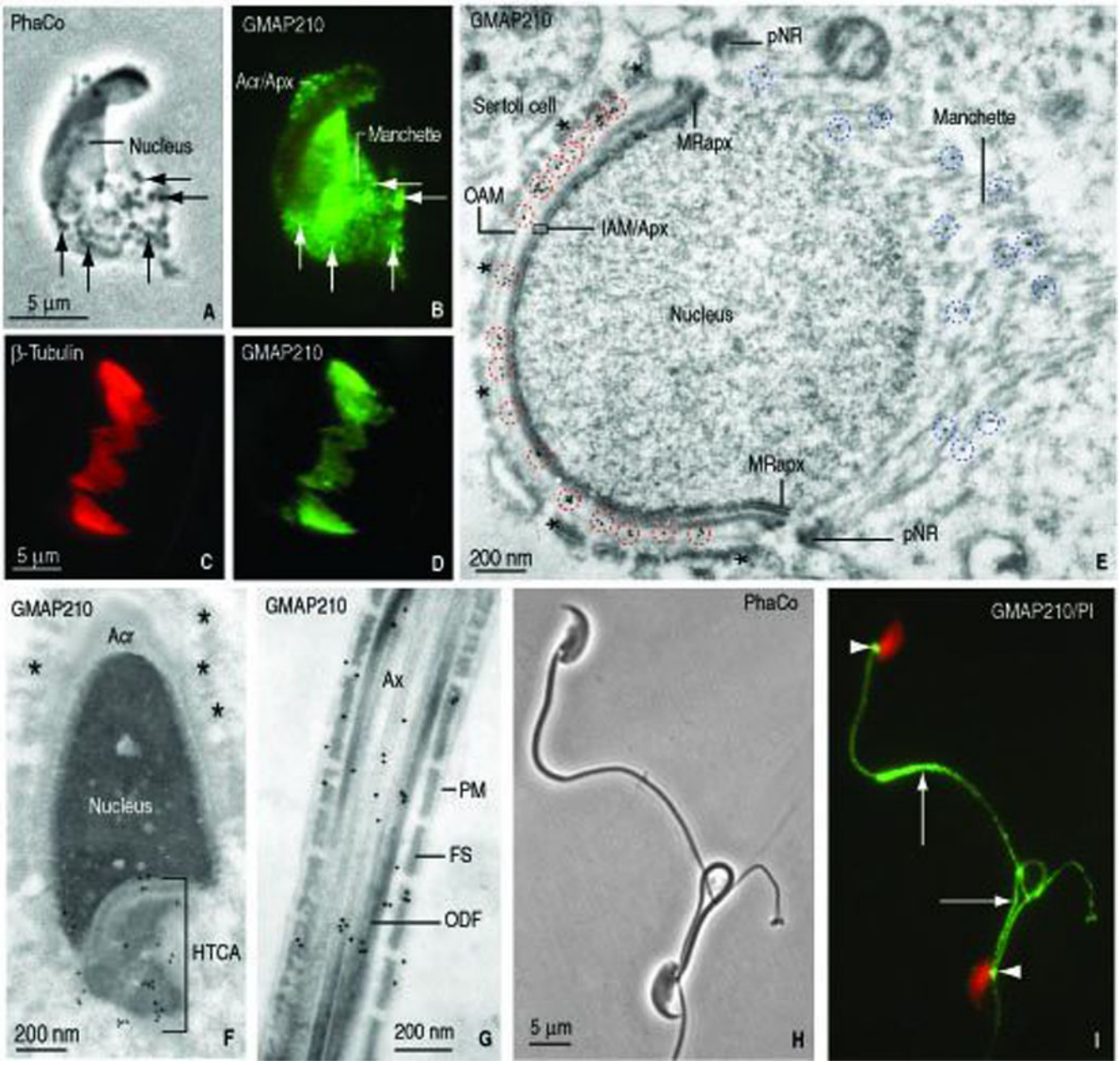

FIGURE 3.

Localization of GMAP210 in elongating spermatids and fractionated manchettes (rat) and epididymal sperm (mouse). **A**. Phase contrast microscopy of an elongating rat spermatid (panel A, **PhaCo**; step 10) shows an elongating head and the associated manchette with granular material (**arrow**). **B**. GMAP210 immunofluorescence is seen in the acrosome-acroplaxome (**Acr/Apx**) and the manchette. The Golgi has already migrated to the caudal cytoplasmic region of the spermatid (not shown). **C–D**. β-tubulin and GMAP210 stained fractionated manchettes from rat spermatids. **E**. Immunogold electron microscopy localization of GMAP210 along the outer acrosome membrane (**OAM**), the inner acrosome membrane-acroplaxome interface (**IAM/Apx**) and microtubules of the manchette. **pNR**,

perinuclear ring of the manchette. **MRapx**, marginal ring of the acroplaxome. The blue dashed circles denote the localization of GMAP210 in the manchette; the red dashed circles emphasize the localization of GMAP210 on the acrosome membranes. The **asterisks** indicate bundles of F-actin in the apical ectoplasmic region of a Sertoli cell. The bundles are closely apposed to the elongating acrosome-acroplaxome-nucleus. **F**. Elongating spermatid (rat, step 16). GMAP210 is localized in the head-tail coupling apparatus (HTCA) but not along the acrosome (**Acr**) membranes and the subjacent acroplaxome. The **asterisks** indicate bundles of F-actin in an adjacent Sertoli cell. **G**. Principal piece of the tail of an elongating spermatid. GMAP210 is seen along the axoneme (**Ax**), outer dense fibers (**ODF**) and portions of the fibrous sheath (**FS**). **PM**, plasma membrane. **H.** Epididymal mouse sperm (phase contrast microscopy, PhaCo). **I**. GMAP210 is not visualized in the sperm head but is seen in the HTCA (**arrowheads**) and the tail (**arrow**s).

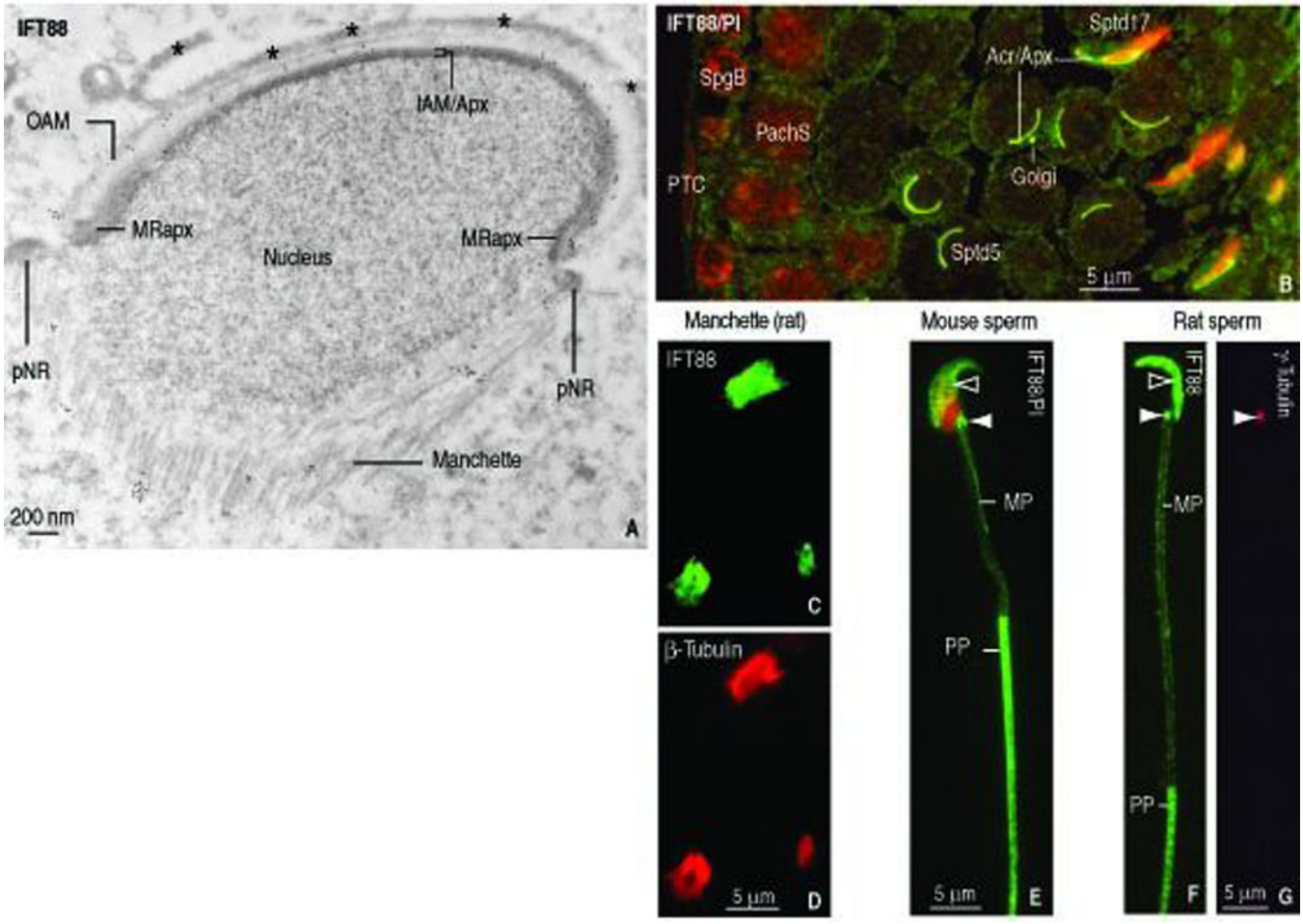

FIGURE 4.

Localization of IFT88 in elongating spermatids, fractionated manchettes (rat), epididymal sperm (mouse and rat) and rat seminiferous epithelium. **A**. Immunogold electron microscopy depicts IFT88 along the outer acrosome membrane (**OAM**), the inner acrosome membrane-acroplaxome (**IAM/Apx**) and microtubules of the manchette. The **asterisks** indicate bundles of F-actin in the apical ectoplasmic region of a Sertoli cell. **pNR**, perinuclear ring of the acroplaxome. **MRapx**, marginal ring of the acroplaxome. **B**. Indirect immunofluorescence of rat seminiferous epithelium (stage V of spermatogenesis). IFT88 is seen in the Golgi and acrosome-acroplaxome (**Acr/Apx**) region of round spermatids (step 5) and elongated spermatids (step 17). No IFT88 immunoreactivity is seen in peritubular cells (**PTC**), spermatogonial B cell (**SpgB**) and pachytene spermatocytes (**PachS**). **C–D**. IFT88- (panel C) in β-tubulin- (panel D) stained fractionated manchettes from rat spermatids. **E**. Mouse sperm. IFT88 is seen in the acrosome-acroplaxome (**open arrowhead**) and the HTCA (**solid arrowhead**). The nucleus is stained red with propidium iodide. The principal piece (**PP**) of the tail displays stronger IFT88 immunoreactivity when compared to the middle piece (**MP**). **F**. The localization of IFT88 in rat sperm tail and HTCA is similar to mouse sperm (panel E). **G**. Same rat sperm shown in panel F stained with γ-tubulin to identify the centrosome, shown in panel F stained with IFT88 antibody (**solid arrowheads**).

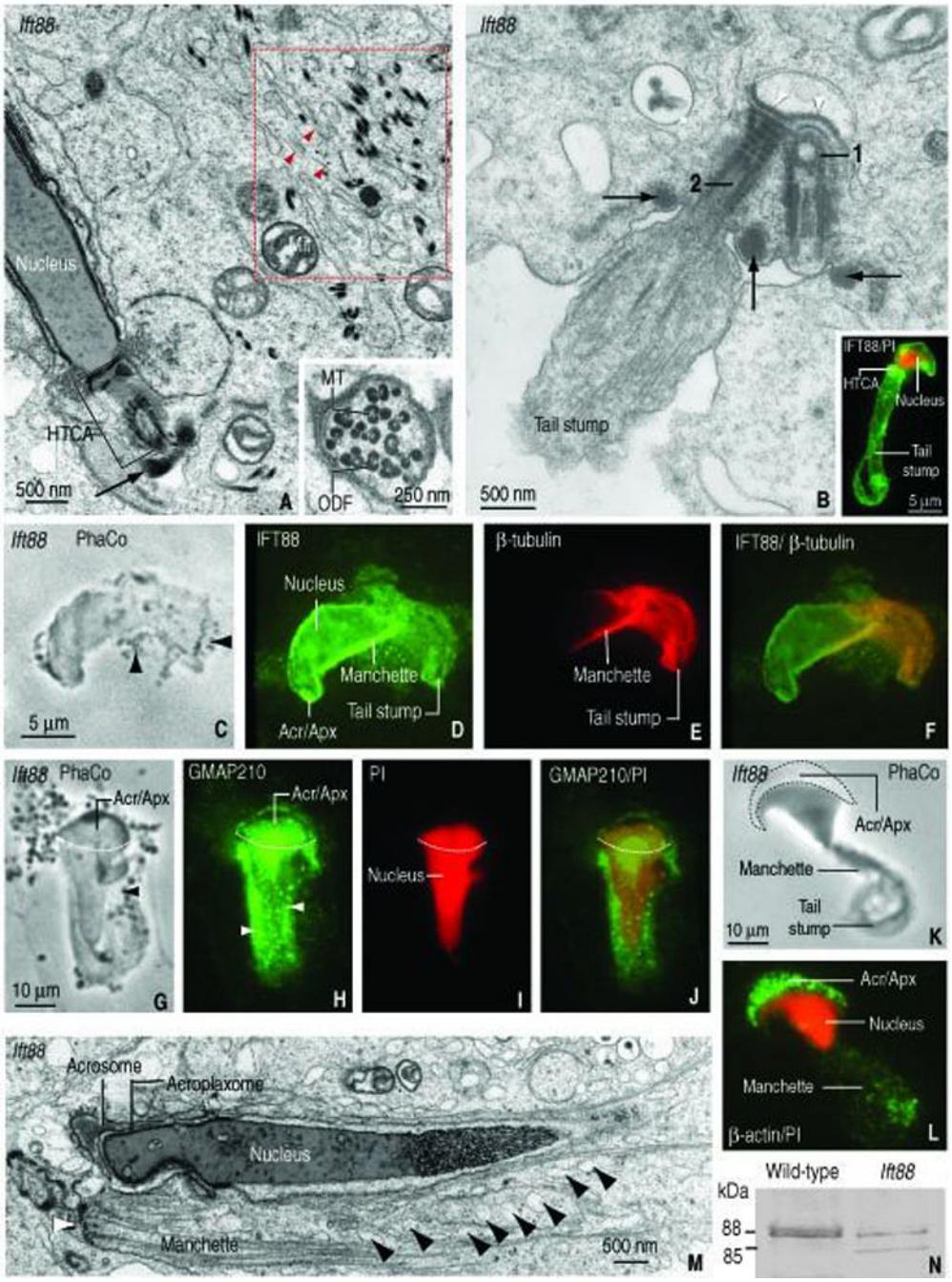

FIGURE 5.

Structural features of spermatids of the *Ift88* mutant mouse. **A**. Elongated spermatid showing a gap between the spermatid nucleus and the head-tail coupling apparatus (**HTCA**) occupied by an amorphous material. The **arrow** indicates the position of the annulus. The **red dashed box** shows dispersed outer dense fiber material, microtubules (**red arrowheads**) and adjacent mitochondria (**Mit**). The **inset** shows clustered outer dense fibers (**ODF**) associated with single microtubules (**MT**). **B**. An abortive spermatid tail displays a pair of HTCAs associated to a single implantation fossa (**white arrowheads**) and three dense

masses (**arrows**) corresponding to annulus material. The proximal centriole (**1**) and distal centriole (**2**) are indicated. The tail stump consists of randomly arranged microtubules. The **inset** illustrates a similar elongated spermatid of the *Ift88* mutant stained with anti-IFT88 serum. Most of the immunoreactivity is observed in the head, surrounding the propidium iodide-(**PI**) stained nucleus and from the HTCA (**HTCA**) down to the tail stump. **C–F**. Elongating spermatid (phase contrast microscopy, **PhaCo**, panel C). IFT88 is seen in the acrosome-acroplaxome, the manchette and the tail stump (panel D). Staining with β-tubulin identifies microtubules of the manchette and the tail stump (panel E). Panel F is a merge of panels D and E. **G**. Elongating spermatid showing the acrosome-acroplaxome and the manchette, the latter with associated vesicles (**arrowhead; PhaCo**). **H**. GMAP210 in the acrosome-acroplaxome complex (**Acr/Apx**) and manchette. Punctuate fluorescent material, regarded as vesicles, is seen in the manchette (**arrowheads**). **I**. The PI red staining delineates the abnormal nucleus shape of the elongating spermatid. **J**. Merge of panels H and I. The **dashed line** in all panels represents the boundary of the acrosome-acroplaxome complex. **K–L**. The PhaCo panel K illustrates an elongating spermatid of the mutant with anormal head shaping and a tail stump. The panel L illustrates the localization of β-actin in the Acr/Apx region and in the manchette region, above the tail stump. **M.** Electron microscopy of an elongated spermatid of the *Ift88* mutant. The acrosome, acroplaxome and nucleus are indicated. The **white arrowhead** points to the ectopic location of the perinuclear ring of the manchette. The **black arrowheads** show several vesicles associated with microtubules of the manchette. **N**. Immunoblotting illustrating IFT88 protein patterns in testes of *Ift88* mutant and the wild-type mice. An 88 kDa form in wild-type testis, regarded as mature IFT88, contrasts with the protein doublet seen in the *Ift88* mutant. The upper band of the doublet (88 kDa) is regarded as mature protein; the lower band (85 kDa) is interpreted as a truncated form.

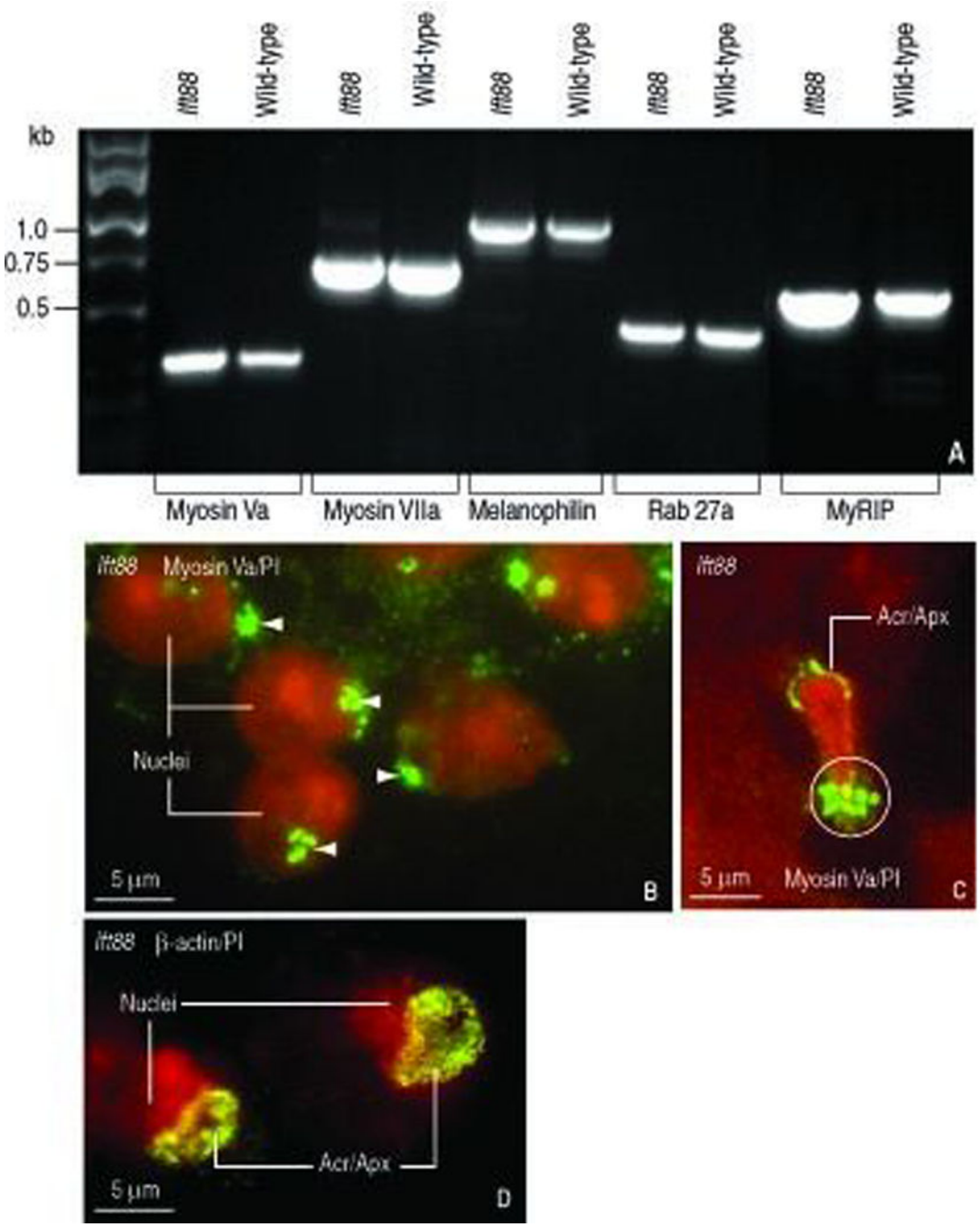

FIGURE 6.

Transcript of the actin-based transport system and adaptor proteins in testes of wild-type and *Ift88* mutant mice and localization of myosin Va in *Ift88* mutant spermatids. **A**. Testes of wild-type and *Ift88* mutant mice express myosin Va and VIIa, the adaptor proteins melanophilin and myRIP (for myosin Va-Rab27a interacting protein) and the vesicle receptor Rab27a. **B**. Proacrosomal vesicles stained with myosin Va (**white arrowheads**) tether to the acrosome-acroplaxome region. Round spermatid nuclei are stained red with propidium iodide (**PI**). **C**. Elongating spermatid showing a myosin Va-stained acrosome-

acroplaxome complex (**Acr**/**Apx**) capping the abnormally shaped PI-stained nucleus. The **white circle** indicates the clustering of myosin Va-stained vesicles at the caudal portion of the manchette. **D**. Localization of β-actin in the Acr/Apx region of round spermatids of the *Ift88* mutant.

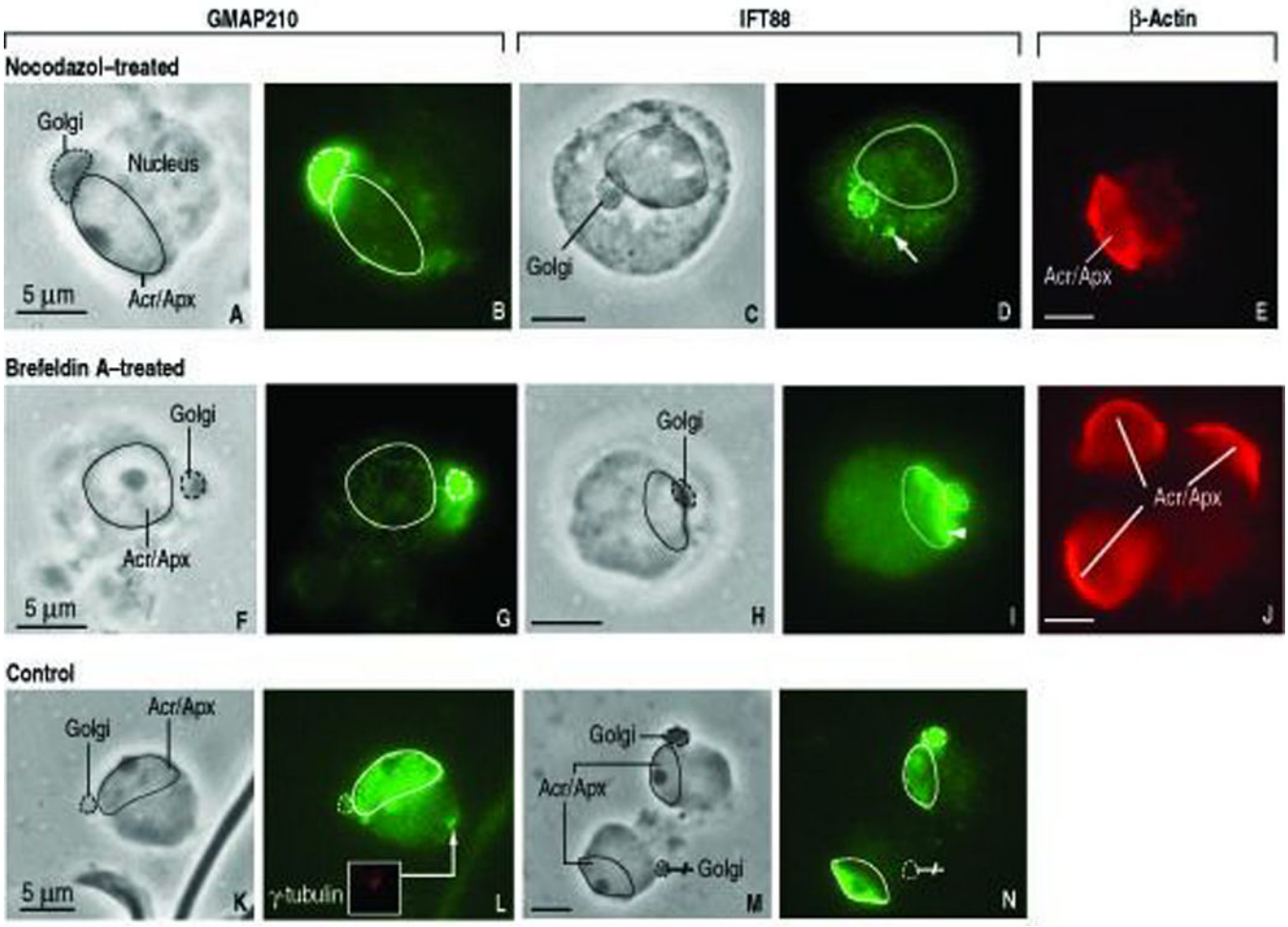

FIGURE 7.

In vitro effect of nocodazole (10 μM, 2 hs) and Brefeldin-A (10 μg/ml, 20 min) on the distribution of GMAP210 and IFT88 in round spermatids (rat; step 6). In all panels, a **dashed line** indicates de outline of the Golgi and a **full line** denotes the perimeter of the acrosome-acroplaxome (**Acr/Apx**) complex. Panels A, C, F, H, K and M are the corresponding phase contrast microscopy (**PhaCo**) images to the immunofluorescence microscopy. **A–B**. Nocodazole confines the localization of GMAP210 in the Golgi (panel B) accompanied by a significant decrease of specific immunoreactivity in the acrosome-acroplaxome complex. **C–D**: IFT88 immunoreactivity (panel D) is concentrated in the Golgi and in adjacent dotted material regarded as fragmented vesicles (**arrow**) following exposure to nocodazole. **F–G**. Brefeldin-A effect on GMAP210 distribution is similar to nocodazol (compare panel G with panel B). **H–I**. Brefeldin-A effect on IFT88 immunoreactivity (panel I) is similar to nocodazole (compare panel I with panel D) except that the immunoreactive fragmentation pattern is seen along the acrosome-acroplaxome margin. **K–L**. Control (DMSO vehicle only; 2 hs). **L**. GMAP210 immunoreactivity in Golgi, Acr/Apx and the centrosome (**inset**: γ-tubulin staining of the centrosome). **M–N**. Control (ethanol vehicle only; 20 min). **N**. IFT88 in Golgi and the acrosome-acroplaxome complex. In one of the spermatids, the migrating Golgi (**crossed pointer**) lacks IFT88, in contrast to the Acr/Apx.

Panels **E** and **J** are β-actin control panels for the nocodazol and Brefeldin–A experiments. The localization of β-actin in the Acr/Apx is nor affected.

TABLE 1

Primers (Mouse and Rat) Used in RT-PCR Experiments

Rat		
GMAP-210	Forward	GATTGCGCGACCACCTCTTAGAGTC
	Reverse	CCTGCCCTGGATTCCGCTGTAT
Actin	Forward	CAAACAGGAGCAGCCAGGCGAGAAC
	Reverse	GATGTCATGGATCTTCATGGGTTC
Mouse		
Myosin Va	Forward	GGCGCCATCACCCTAAACA
	Reverse	GTGCGGATAAATGAAACTGAGACC
Myosin VIIa	Forward	CCGCTTTGGCTTCTCCCTCTACAT
	Reverse	CCGGCCCGATTGACAAGTAGCA
Melanophilin	Forward	AGACCAGCCCCTCAACAGCAAAAA
	Reverse	TCTCAGTAACGCGGGAAGAAAGAT
Rab27a	Forward	ACCTCGGGATCCATCTGTAACG
	Reverse	TTCCCCCCACCCCCAAACTCA
MyRIP*	Forward	GGCCCCTCCAGGACGACACA
	Reverse	CCGGCTGCCTGAGGGTTGAAT

*Myosin-Rab27a interaction protein